24 μm Detections of Circum(sub)stellar Disks in IC 348: Grain Growth and Inner Holes?

James Muzerolle[1], Lucía Adame[2], Paola D'Alessio[3], Nuria Calvet[4], Kevin L. Luhman[5], August A. Muench[6], Charles J. Lada[6], George H. Rieke[1], Nick Siegler[1], David E. Trilling[1], Erick T. Young[1], Lori Allen[6], Lee Hartmann[4,6], S. Thomas Megeath[6]

ABSTRACT

We present observations of six late-type members of the young cluster IC 348 detected at 24 μm with the Multiband Imaging Photometer for *Spitzer* (MIPS). At least four of the objects are probably substellar. Combining these data with ground-based optical and near-infrared photometry and complementary observations with the Infrared Array Camera (IRAC), we have modeled the spectral energy distributions using detailed models of irradiated accretion disks. We are able to fit the observations with models using a range of maximum grain sizes from ISM-type dust to grains as large as 1 millimeter. Two objects show a lack of excess emission at wavelengths shortward of 5.8-8 μm but significant excess at longer wavelengths, indicative of large optically thin or evacuated inner holes. Our models indicate a inner hole of radius $\sim 0.5 - 0.9$ AU for the brown dwarf L316; this is the first brown dwarf with evidence for an AU-scale inner disk hole. We examine several possible mechanisms for the inner disk clearing in this case, including photoevaporation and planet formation.

Subject headings: accretion disks, brown dwarfs, stars: pre-main sequence, circumstellar matter

[1]Steward Observatory, 933 N. Cherry Ave., The University of Arizona, Tucson, AZ 85721

[2]Instituto de Astronomía, UNAM, Ap. P. 70-264, Ciudad Universitaria, 04510, México, D.F., México

[3]Centro de Radioastronomía y Astrofísica, Ap. P. 72-3 (Xangari), 58089, Morelia, México

[4]University of Michigan, 825 Dennison Building, 501 E. University Ave., Ann Arbor, MI 48109-1090

[5]Department of Astronomy and Astrophysics, The Pennsylvania State University, University Park, PA 16802

[6]Harvard-Smithsonian Center for Astrophysics, 60 Garden St., Cambridge, MA 02138

1. Introduction

Brown dwarfs have been found in increasingly large numbers, particularly in young star-forming regions where their larger luminosities and effective temperatures make them easier to detect. Observations of young substellar objects provide important clues to understanding how brown dwarfs themselves form and, more generally, the nature of the initial mass function. Of particular interest is the study of circumsubstellar disks. Since disks are the primary conduits of accretion onto stars and the likely birthplaces of planetary systems, characterization of disks around brown dwarfs in comparison to their stellar counterparts is key to constraining formation mechanisms and exploring the range of conditions under which planets may form.

Recent investigations by many groups have revealed strong evidence that disk accretion is an important mechanism in brown dwarf formation, apparently identical to the processes that operate in higher-mass T Tauri and Herbig Ae/Be stars. A remarkable similarity exists among objects of widely different masses in terms of both optical and infrared properties associated with the disk accretion process. A wealth of permitted emission lines such as HI Balmer are common in substellar objects; high-resolution spectroscopy reveals these to be broadened by ballistic infall of gas as expected in magnetospheric accretion scenarios (e.g. Mohanty et al. 2005; Muzerolle et al. 2005). Disk mass accretion rates ($\dot{M}$) have been measured for brown dwarf disks using a variety of methods including optical veiling (White & Basri 2003), Hα profile modeling (Muzerolle et al. 2000, 2003a, 2005), near-infrared emission lines (Natta et al. 2004), and the Ca II triplet (Mohanty et al. 2005). The derived values are extremely small, typically $\lesssim 10^{-10} M_{\odot}\,\mathrm{yr}^{-1}$, demonstrating that most if not all disks around low-mass objects must be irradiation-dominated.

Near-infrared excess indicative of optically thick circumstellar disks has been detected around many young substellar objects, although often at a marginal level (e.g. Luhman 1999; Muench et al. 2001; Jayawardhana et al. 2003; Liu et al. 2003). Because of the low luminosities of the central sources, the disk excess produced by irradiation is very small and difficult to measure at K-band and in many cases even at L-band. Thus, observations at longer wavelengths are necessary to find and characterize disk emission in detail. Mid-infrared observations such as ground-based 10 μm photometry (Apai et al. 2004; Mohanty et al. 2004), ISO 6.7 and 14 μm photometry (e.g. Coméron et al. 1998, 2000), and photometry and spectroscopy with the *Spitzer* Space Telescope (Furlan et al. 2005; Luhman et al. 2005a,b) have revealed significant excess emission around dozens of known young objects near and below the hydrogen burning limit. The shape of the infrared spectral energy distributions (SEDs) of these brown dwarf disks is qualitatively similar to that of stellar disks (e.g. Natta & Testi 2001), with suggestions of a wide range of substellar disk structure

and dust properties (Natta et al. 2002; Pascucci et al. 2003; Mohanty et al. 2004; Apai et al. 2004). Further observations such as these are crucial to determining the properties and complete statistics of brown dwarf disks in star forming regions and young clusters.

Here, we present detections of very low-mass and substellar members of the 1-3 Myr-old cluster IC 348 with the 24 μm channel of the Multiband Imaging Photometer for *Spitzer* (MIPS). These data are part of a larger, more comprehensive *Spitzer* GTO imaging study of the cluster (Lada et al. 2005), a prime target since its stellar and substellar population has been well-characterized from the ground (e.g. Luhman et al. 2003). The MIPS observations provide the longest-wavelength infrared photometric measurements of brown dwarfs to date, and thus potentially allow much more stringent constraints on brown dwarf disk structure than heretofore possible. Six objects of spectral type M6 and later, near and below the substellar limit, are detected at 24 μm , exhibiting emission in excess of expected photospheric levels and clearly indicative of emission from circum(sub)stellar disks. In combination with complementary ground-based optical and near-infrared and *Spitzer* Infrared Array Camera (IRAC) observations, we present full SEDs from $\lambda \sim 0.8$ to 24 μm for these six objects. We calculate models of irradiated accretion disk emission including appropriate (sub)stellar parameters, and examine their capabilities and limitations in describing the observed SEDs and constraining disk properties such as surface flaring, inner holes, and dust properties.

2. Observations

We have measured 24 μm photometry from our GTO observations of IC 348 taken in February 2004 with MIPS (Rieke et al. 2004). The cluster was mapped using scan mode with 12 scan legs of length 0.5 degrees and half-array cross-scan overlap, resulting in a total map size of about 0.5 x 1.5 degrees including overscan. The total effective exposure time per point is about 80 seconds. Data at 70 and 160 μm were taken simultaneously; however, we do not consider these here since the sensitivity limits and strong background emission preclude detection of anything but the brightest mid-infrared sources.

The 24 μm images were processed using the MIPS instrument team Data Analysis Tool, which calibrates the data and applies a distortion correction to each individual exposure before combining into a final mosaic (Gordon et al. 2005). Point source photometry was performed on the mosaicked image using PSF fitting with *daophot*. The 3-sigma detection limit is on average roughly 1 mJy, as high as 10 mJy in the central regions of the cluster where the background is strong and highly structured, and as low as 0.7 mJy in the lowest-background regions of the map. In most cases the measurement errors are dominated by the 10% uncertainties in the flux calibration.

3. Analysis

3.1. 24 μm properties

The membership of IC 348 has been well-characterized in various ground-based optical and near-infrared investigations (Luhman et al. 2003 and references therein). The low-mass pre-main sequence population has been confirmed primarily via spectroscopic indicators of youth such as Hα emission, Li absorption, and various gravity sensitive features. Here we restrict our analysis to cluster members near or below the substellar limit, selecting only objects with spectral types M6 or later. This cut-off roughly corresponds to a mass of about 0.1 $M_{\odot}$ at the age of IC 348 (roughly 1-3 Myr) using the pre-main sequence evolutionary tracks of Baraffe et al. (1998) and the temperature scale of Luhman et al. (2003).

Figure 1 shows the positions of the 36 known $\geq$M6 members superposed on the 24 μm image. Six of these were clearly detected and measurable at 24 μm , while of the remainder, one is an unresolved companion to a much higher-mass cluster member, and two others are marginally detected but unmeasurable due to significant background contamination. The (sub)stellar properties of the detected objects are listed in Table 1; the IRAC and MIPS fluxes are listed in Table 2. Herein, we refer to these 6 objects as the low-mass/substellar 24 μm sample (four objects are below the substellar limit according to the Baraffe tracks). The matching to optical/near-infrared positions in all cases is within about 1 arcsecond, consistent with the typical pointing accuracy of MIPS. Confusion with red background objects is extremely unlikely; in the flux range of the sample, extragalactic source counts predict roughly 1-10 sources per square degree (Papovich et al. 2004), resulting in a chance alignment probability of $\sim 10^{-6}$. The 24 μm detections lie primarily at the outskirts of the cluster, probably reflecting a bias towards lower-background regions of the map where our detection limits are lower.

The 24 μm fluxes of our low-mass sample are all strongly in excess of expected photospheric levels by factors of 100 or more, not surprising since the sensitivity limit of our observations is too high to detect photospheric or weak excess emission from M dwarfs at the distance of IC 348. The large mid-infrared excess luminosity implied by our observations indicates that these objects all harbor significant optically thick disks. Previous detections of accretion activity on at least 2 of the 6 (L205 and L291; Muzerolle et al. 2003a, Mohanty et al. 2005) corroborate this conclusion. Since the flux at 24 μm is completely dominated by the excess emission, it offers optimal new constraints on the properties of disks around very low-mass objects.

Inferences of disk structure are greatly dependent on theoretical models, which, as we will show, can be quite degenerate. However, as an initial guide, we can examine the observed

fluxes in comparison with other higher-mass objects and simple theoretical expectations. In Figure 2 we show the ratio of the flux at 24 μm to the flux at 4.5 μm measured from complementary IRAC observations (Lada et al. 2005; Luhman et al. 2005) as a function of the 24 μm flux. We chose 4.5 μm as a reference since in most cases it is the shortest wavelength with relatively unambiguous excess emission in the lowest-mass objects (though there are a few exceptions; see below). The low-mass/substellar sample spans a range in the flux ratio of about 0.5 dex, roughly a factor of 50-100 above the theoretical flux ratio of an M6.5 photosphere. In comparison, we also plot a flux ratio upper limit for a flat, optically thick and geometrically thin disk. All 6 low-mass/substellar 24 μm detections lie well above this line, suggesting that the disks are not "flat" but likely have some amount of flaring. However, detailed modeling is required to draw more definitive conclusions, as we discuss in the next section.

As a further comparison, Figure 2 shows the median flux ratio of IC 348 late-type stellar members in the range M4-M5 which exhibit excesses indicative of optically thick disks (Lada et al. 2005). Four of the six objects in our low-mass/substellar sample lie within the one-sigma range of this median ratio, suggesting no significant differences in disk surface structure for these particular objects. The other objects, L316 and L30003, exhibit significantly higher flux ratios than the M4-M5 stellar median. A closer look at the SED of L316, shown in Figure 3, reveals a lack of excess emission compared to the photosphere at wavelengths shorter than $\sim$8 μm . A similar result is seen in the SED of L30003, but with a cut-off at a slightly shorter wavelength. This behavior indicates a significant depletion of small dust grains, or perhaps no material at all, within the inner $\sim$ 1 AU of the disk. Truncated inner disks associated with the magnetospheric disruption or dust destruction radius have been previously diagnosed in T Tauri disks on the basis of the near-infrared excess spectrum (Muzerolle et al. 2003b), interferometry (e.g. Akeson et al. 2005), and CO gas emission lines (Najita et al. 2003). Such truncation radii are typically $<$ 0.1 AU for typical low-mass (sub)stellar parameters. However, the inferred "hole" sizes for L316 and L30003 are much larger, more akin to "transition" disks found around higher mass stars such as CoKu Tau/4 (D'Alessio et al. 2005) and TW Hya (Calvet et al. 2002), and thus require a different creation mechanism. We examine several possibilities in detail in section 4.2.

3.2. SED modeling

We next compare the observed infrared emission of each of the low-mass/substellar objects in our sample with detailed vertical structure models of irradiated accretion disks. The assumptions, equations and description of the method used to calculate the disk structure

and emergent intensity are given in D'Alessio et al. (1998, 1999, 2001); we defer the details to these papers. In brief, the disks are assumed to be in steady-state, with dust and gas well-mixed and thermally coupled and the mass accretion rate uniform throughout the entire disk. We adopt a viscosity parameter $\alpha = 0.01$, as is typically assumed for T Tauri disks (but not well-constrained; see e.g. Hartmann et al. 1998). The dust grain size distribution is given by the standard power law $n(a) \sim a^{-3.5}$ (Mathis, Rumpl, & Nordsieck, 1977), with minimum grain size $a_{min} = 0.005$ μm and maximum grain size varied to be either $a_{max} = 0.25$ μm (consistent with ISM dust; D'Alessio et al. 1999) or $a_{max} = 1$ mm (the maximum grain size of the model that best fits the median SED of classical T Tauri stars in Taurus; D'Alessio et al. 2001) as a preliminary exploration of dust grain growth within these disks. The inner disk radius R_{wall} for a "*normal*" disk is given by the dust sublimation radius R_{sub} where $T_{sub} \sim 1400$ K. In a few cases, we also consider larger inner radii ("*truncated*") as the observed near-infrared emission dictates. We include the emission of a vertical wall at the inner edge, where the dust has been heated by frontal irradiation from the central object (see Muzerolle et al. 2003b and D'Alessio et al. 2005 for details of the treatment). If an object is actively accreting and has a dust sublimation radius larger than the corotation radius (as is usually the case), a pure gaseous disk must be present interior to R_{sub}. Since emission from this component is negligible at low accretion rates (Muzerolle et al. 2004), we neglect it in our models. The maximum disk radius is fixed at 100 AU; no constraints on disk radii are available for the objects under study here, but in any case the model SEDs are not very sensitive to this parameter in the wavelength range we consider.

For comparison to the observed SEDs, we adopted (sub)stellar parameters as shown in Table 1 and a distance to IC 348 of 315 pc. The observed fluxes were corrected for extinction according to the Mathis (1990) reddening law given the empirical A_V values shown in Table 1. For each object, we explored a range of inclination angles to the line of sight, and three mass accretion rates (10^{-12}, 10^{-11}, and 10^{-10} $M_\odot\,\mathrm{yr}^{-1}$) which are in the typical range for young very low mass stars and brown dwarfs (Muzerolle et al. 2003a, 2005). The height of the inner disk wall was then adjusted to fit the observed flux in the 2-8 μm range. Table 3 shows the input parameters of the best fit models for each observed SED and the resultant physical parameters of the wall and disk. The SEDs are shown in Figure 4.

For objects L199, L205, L291, and L1707, "*normal*" disk models with a range of a_{max} are capable of reproducing the observed SEDs. The emission arising from the inner disk wall is required in order to match the fluxes in the 2-8 μm range, while the outer disk is only responsible for the emission redward of ~ 10 μm ; Figure 5 shows the relative contributions of the various components of a typical model. We find that a disk with $\dot{M} = 10^{-11} M_\odot\,\mathrm{yr}^{-1}$, $a_{max} = 0.25$ μm , and an inclination angle of 60° provides reasonable fits for L205, L291, and L1707. In the case of L199, we can only match the observed SED with $a_{max} = 0.25$ μm for a

relatively extreme combination of pole-on disk with small accretion rate $\dot{M} = 10^{-12} M_{\odot}\,\mathrm{yr}^{-1}$. Disks with larger maximum grain sizes up to $a_{max} = 1$ mm can also fit the observed SEDs if the accretion rates are increased by one or more orders of magnitude and the inclination angles are changed significantly (nearly pole-on orientations for L205, L291, and L1707 and 60° for L199). To fit the near-infrared fluxes we also have to change the wall height to compensate for the change in model flux as a result of orientation effects (i.e., the wall emission decreases as the inclination becomes more pole-on because of our assumed vertical geometry). The adopted heights are shown in Table 3, along with the expected height given $a_{max} = 0.25$ μm in the wall and equations 5 and 6 from Muzerolle et al. (2004). Figure 5 compares models with the two maximum grain size extrema; the overall disk flux is similar in both models owing to the adjustments in $\dot{M}$ and inclination, but the 10 and 20 μm silicate features, produced in the atmosphere of the outer disk, are markedly weaker for $a_{max} = 1$ mm (see also D'Alessio et al. 2001). Spectra of these features are obviously important to discriminate between the two cases.

As already mentioned, objects L316 and L30003 exhibit a lack of excess emission at wavelengths smaller than $5.8 - 8$ μm , indicating a lack of hot dust. We could not obtain a good fit with any "normal" disk model, thus, we have calculated the emission from a disk *truncated* at radii larger than the dust sublimation radius, following the treatment of Muzerolle et al. (2003b) and D'Alessio et al. (2005). The inner wall in this case is the transition between an optically thin or completely evacuated hole and an optically thick outer flared disk which contributes to the SED only at longer wavelengths, generally > 10 μm . Again we assume that $a_{max} = 0.25$ μm ; the maximum grain size is varied between 0.25 μm and 1 mm for the outer disk only. Figure 6 shows the emission components for one such model run for L316. The emission redward of 8 μm is dominated entirely by the vertical wall, which is located near 1 AU and hence has a significantly lower surface temperature (~ 200 K) than the dust sublimation point. We have set $\dot{M} = 10^{-12}$ $M_{\odot}$ yr^{-1} for models of both L316 and L30003, but observational constraints are lacking. This level is probably an upper limit for L316 since its small Hα equivalent width (3 Å) indicates either very weak or completely blocked accretion onto the central object.

4. Discussion

4.1. Grain Growth and Dust Settling?

Comparisons of disks around low-mass stars and brown dwarfs can in principle provide clues to differences or similarities in formation mechanisms, as well as put limits on the possibility of planet formation. Mid-infrared measurements probe dust emission from the

terrestrial zone of disks and provide a useful point of comparison for investigating bulk dust properties. Of particular interest has been the detection of infrared signatures of disk evolution via grain growth and settling. Evidence for such processes has been inferred for "mature" T Tauri disks at ages of up to 5-10 Myr (Calvet et al. 2005a; Sicilia-Aguilar et al. 2005). As mentioned in the introduction, previous measurements of thermal dust emission from a small number of brown dwarfs have indicated a range of disk properties, from surface flaring and dust grain sizes typical of most 1 Myr-old T Tauri stars to flatter disks with evidence for significant dust grain growth and settling towards the disk midplane. These inferences are based primarily on observed fluxes out to 14 μm and rough silicate emission strengths from narrow-band 10 μm imaging (Apai et al. 2004; Mohanty et al. 2004; Sterzik et al. 2004). Our 24 μm observations potentially offer an even more sensitive indicator of the disk surface geometry since they probe a more distant range of disk radii (roughly 0.5-1 AU for a central substellar object) where the disk height is up to 30% greater (D'Alessio et al. 1999).

The flux ratios shown in Figure 2 suggest that the disks in our sample are not flat but must have some amount of flaring, to a degree not dissimilar to that seen in the low-mass stellar population of IC 348 in general. Lada et al. (2005) compare stellar SEDs as a function of spectral type and find that the latest-type stars (>M4) with disks exhibit steeper spectral slopes than seen in earlier-type stars with disks, possibly indicating a higher frequency of dust settling around lower-mass objects. However, our disk model comparisons indicate that we cannot easily constrain the dust properties for most of the low-mass/substellar sample. Without additional information such as the mass accretion rate or the 10 and 18 μm silicate features, the observed excess emission out to 24 μm can be explained by a wide range of maximum dust grain sizes, from ISM-type to as large as 1 mm. Observational constraints on the disk mass accretion rates are available only for L205 ($\dot{M} = 10^{-10} M_{\odot}\,\mathrm{yr}^{-1}$; Muzerolle et al. 2003a) and L291 (an upper limit of $\dot{M} < 10^{-11} M_{\odot}\,\mathrm{yr}^{-1}$; Mohanty et al. 2005). These would seem to argue against the $a_{max} = 0.25$ μm model for L205 since the model accretion rate is a factor of 10 lower. If this is the case, we may be seeing evidence of grain growth in the L205 disk. For object L199, the $a_{max} = 0.25$ μm model only fits for rather extreme values of $\dot{M}$ (small) and inclination (pole-on), which may not be realistic particularly since pole-on orientations should be statistically rare. Similarly, the $a_{max} = 1$ mm models may not hold for L291 and L1707 since they also require pole-on orientations.

One suggestion of dust settling may be seen in the vertical heights of the inner disk wall component of the models. The heights required to match the short-wavelength excess of objects L199 and L205 are factors of 1.5-2 smaller than the expected heights derived from equation 6 of Muzerolle et al. (2004). It is possible that grain growth and settling in the inner disk can result in smaller than expected wall heights. However, the exact values constrained

by our models are limited by uncertainties in the level of the underlying photosphere (see Table 3) as well as the uncertain structure of the inner wall. Models incorporating the wall with the outer disk in a self-consistent manner, including the effects of dust settling to the disk midplane, must be explored before definitive conclusions can be made. Again, mid-infrared spectra covering the silicate features are also crucial observational constraints that should be obtained. We further caution that all the "normal" disk models presented here implicitly assume that the wall radius is at the dust sublimation point. Given the cool and faint radiation fields of very low-mass objects, the sublimation radius is quite small (Table 3) and may in fact be smaller than the radius at which the (sub)stellar magnetosphere truncates the gas disk. If this is the case, the dust edge should then be at the magnetospheric radius and can have a dust temperature less than 1400 K, yielding weaker near-infrared excess emission (a lower temperature might also provide a better fit to the spectral slope at the IRAC bands in L205). Since estimates for the magnetospheric truncation radii are highly uncertain, we leave this complication for a future study.

We must also point out that all of the models we consider here assume the same constant value of the viscosity parameter α. The model SED at $\lambda > 10$ μm can be modified significantly if α is changed by just an order of magnitude. There is no theoretical nor observational impediment, at this time, to adopting different values of α. For smaller values, the disk density will increase assuming a constant $\dot{M}$, since $\Sigma \propto \frac{\dot{M}}{T_c \alpha}$, where T_c is the temperature at the disk midplane. If the density increases, the height of the irradiation surface, defined as the height where the mean optical depth to the (sub)stellar radiation is unity, also increases. The higher the irradiation surface, the larger the fraction of incident (sub)stellar flux is intercepted and reprocessed by the disk. On the other hand, the mean opacity to the (sub)stellar radiation is smaller with increasing a_{max} from ISM-like values to millimeter sizes. Thus, different combinations of $\dot{M}$, α, and a_{max} can fit the same SED. A full exploration of the effects on the structure of disks around very low mass objects produced by varying α are beyond the scope of this work. In any case, 10 μm spectra and millimeter observations are required for a more rigorous test of the grain growth hypothesis for objects L199 and L205. Models including the effects of dust settling to the disk midplane should also be explored.

4.2. Inner Disk Clearing

Two objects, L316 and L30003, show evidence for inner disk clearing beyond what could be explained by magnetospheric truncation or the dust destruction radius alone. L316 is the first young brown dwarf known to exhibit a significant inner disk "hole". This result has potentially significant impact on our understanding of disk clearing mechanisms since the

low object masses provide stringent constraints on theoretical models previously proposed to explain similar "transition" disks around higher-mass young stars. We discuss two possibilities, photoevaporation by the UV flux of the central object and clearing via grain growth or planet formation.

4.2.1. Photoevaporation

Clarke et al. (2001), building on the pioneering work of Hollenbach et al. (1994), first proposed a photoevaporative wind as a means of producing inside-out clearing of circumstellar accretion disks. In brief, the model treats mass loss from the disk surface as a result of photoevaporation caused by the impinging UV radiation of the central star. This loss occurs beyond a characteristic "gravitational radius" (R_g) that depends on the mass of the central object and the sound speed of the photoionized gas. As the disk viscously evolves with time its mass accretion rate decreases steadily; once the accretion rate drops below the photoevaporative mass loss rate, the disk experiences a net loss of material outside R_g. A gap quickly forms at R_g ($\sim 5 - 10$ AU for typical T Tauri stellar parameters), and the continuing mass loss prevents replenishment by accreting material from outside. The inner disk, now decoupled at R_g, drains onto the star in a viscous time (a few times 10^5 yrs for typical T Tauri stars), leaving a hole in the disk of size R_g. The outer disk then continues to evaporate away more slowly.

The main difficulty with this model has been the origin of sufficient UV flux. Matsuyama et al. (2003) showed the excess hot continuum produced by typical T Tauri accretion shocks does not produce enough UV flux, particularly when the decrease in mass accretion rate with time expected by viscous evolution is folded in. We can now place more stringent constraints on the timescales for this process to operate by inference from the very low-mass objects which show inner disk clearing. In particular, the hole radius we infer for object L316 with the $a_{max} = 1$ mm model is similar to the gravitational radius $R_g = GM_*/a^2 = 0.5$ AU, where a is the sound speed of the ionized gas with assumed $T = 10^4$ K. Ruden (2004) gives useful scaling relations for the photoevaporative mass loss using a framework similar to that of Matsuyama et al., assuming that the accretion shock is the only source of significant EUV photons and emits blackbody radiation with characteristic temperature 15,000 K. Most applicable for our purposes is the characteristic timescale for disk removal, $t_e = 3.4 \times 10^7\, yr\ (M_{d0}/10^{-2} M_\odot)^{2/3}\, (M/M_\odot)^{-5/6}\, (\alpha/10^{-2})^{-1/3}$, and the total mass removed, $\Delta M_w = 0.3\, M_J\ (M_{d0}/10^{-2} M_\odot)^{2/3}\, (M/M_\odot)^{7/6}\, (\alpha/10^{-2})^{-1/3}$. We adopt an initial

disk mass $M_{d0} = 10\ M_J$ as a plausible upper limit[1], and a viscosity parameter $\alpha = 0.01$. With these assumptions, we estimate that a total of only $\sim 4.7\ M_\oplus$ can be removed via a photoevaporative wind in about 300 Myr, some 300 times longer than the age of the object. Smaller values of α will only increase the evaporative timescale; smaller initial disk masses will decrease the timescale but also vastly decrease the mass removed. Thus, we conclude that a photoevaporative wind generated by UV radiation from a substellar accretion shock cannot have produced the inner disk hole we see in L316. In fact, there may be no accretion shock at all on L316 if accretion has indeed shut off, as its Hα equivalent width seems to suggest (though a resolved line profile would provide a better indicator). An alternative source of the UV flux may arise from the chromosphere; however, it would need to provide a steady flux of $\Phi \gtrsim 10^{40}$ s^{-1} (Ruden 2004), which is difficult to imagine for such a low-mass object. However, measurements of the chromospheric UV flux in young objects of any mass are lacking.

4.2.2. Planetesimal growth and/or planet formation

Significant grain growth and settling in the inner disk may lead naturally to rapid formation of meter or kilometer-sized planetesimals. Models of dust coagulation in protoplanetary disks predict growth at a rate proportional to the square of the orbital period, with faster timescales in the inner disk because of the higher velocities (e.g. Weidenschilling 1997). Recent simulations along these lines by Dullemond & Dominik (2005) demonstrated that small grains can be removed quickly from the inner regions of T Tauri disks, so long as they are not replenished. In fact, the process appears to act too quickly, in less than 1 Myr, and replenishment by aggregate fragmentation from high speed collisions was suggested by Dullemond & Dominik as a way to extend disk lifetimes to agree with observations. Larger scale effects associated with the dissipation of the gas in the disk may also cause planetesimal orbits to shift and create additional collisions since the system will never reach a static state until the gas is gone. Other proposed mechanisms for the removal of small dust grains in disks around low-mass stars, such as corpuscular wind drag (Plavchan et al. 2005), only apply once the gas has completely dispersed. Therefore, the attribution of cleared inner disks to clearing by planet formation brings its own set of complications. It may mean a system of planetesimals akin to the asteroid belt within the cleared inner zone at a time away from major collision

[1]This gives a ratio $M_{disk}/M_* \sim 0.1$, at the high end of the range measured in T Tauri stars and close to the limit for gravitational instability. The only published disk mass measurements for substellar objects are from Klein et al. (2003), who estimated values in the range 0.4-2.4 and 1.7-5.7 M_J for the brown dwarfs CFHT-BD-Tau 4 and IC 348 613, respectively.

events, or it may suggest the very rapid formation of a massive planet within a few AU of the central object, as has been suggested for T Tauri stars with similar evidence for inner disk holes such as TW Hya (Calvet et al. 2002), GM Aur (Rice et al. 2003; Calvet et al. 2005b), and CoKu Tau/4 (D'Alessio et al. 2005).

The case of L316 may illustrate the latter of these possibilities. Accretion has probably ceased altogether, and if so there is likely little or no gas inside the hole. In order to prevent accretion from the outer disk from proceeding through the hole onto the star, dynamical perturbation from a planetary-mass object might be required. Hydrodynamic simulations by Quillen et al. (2004) have shown that planetary companions around young stars can disrupt the inner disk and prevent further accretion from the outer disk if they are sufficiently massive. They estimate this lower limit in the case of the inner disk hole-bearing T Tauri star CoKu Tau/4 using the gap-formation criterion that the ratio of the planetary and primary masses $q \geq 40\,\mathrm{Re}^{-1}$, where the Reynolds number Re is a function of the disk viscosity (Nelson et al. 2000). For the α-disk prescription, $Re = \alpha^{-1}(v_c/c_s)^2$, where v_c is the Keplerian velocity of a particle at a given radius in the disk and c_s is the sound speed at the same radius. In the case of object L316, we adopt an inner hole size of 1 AU, the temperature at the disk edge $T \sim 200$ K, and the Keplerian velocity at the edge given the mass of L316. Assuming $\alpha = 0.01$, we then derive a rough lower limit $M_p \gtrsim 0.8\ M_J$ for the planetary mass necessary to maintain the observed hole.

The initial disk around L316 most likely did not have enough material within 0.5-1 AU to form a planet this large. We have simulated a possible initial disk using a standard model with $\alpha = 0.01$, inner edge at the dust sublimation radius, and a much larger accretion rate of $10^{-9}\ M_\odot\,\mathrm{yr}^{-1}$ (a plausible initial value based on the observed range of accretion rates in brown dwarfs; Muzerolle et al. 2005). The resulting model contains about 2-3 $M_\oplus$ of total dust+gas inside 0.5 AU. However, α is not known; values of $10^{-4} - 10^{-3}$ are theoretically plausible and would give smaller lower limits to the planetary mass necessary to maintain the inner hole, $M_p \gtrsim 2.5 - 25\ M_\oplus$, as well as more mass in the initial disk. A lower α could for instance be indicative of a disk in which the midplane is inactive ("dead zone"; Gammie 1996), with very low or zero equivalent α, and accretion occurs only in an active layer with larger α. The same initial disk model with these smaller values of α results in disk masses within 0.5 AU of up to 60 $M_\oplus$. Thus, a sufficient reservoir of material could have been present around L316 initially for this scenario to hold. However, the mean age of IC 348 members then requires a fast planet formation timescale of a few Myr or less. The surface densities of the initial disk models are too low by several orders of magnitude for the disk instability model of Boss (1997) to apply. More work needs to be done to evaluate whether the traditional models of core formation (or even "super-Earth" formation) via planetesimal collisions can build an object in the mass range we estimate in the time required.

5. Summary

We have reported on the detection at 24 μm of dust emission from 6 very low mass or substellar members of the 1-3 Myr-old cluster IC 348. The amount of excess emission in all cases is consistent with an origin in optically thick disks. In combination with ground-based and *Spitzer* IRAC photometry, we find that the SED shapes of four objects are similar to those of most of the disks around M stars in the same cluster, indicating similar flared disk geometries. Models of irradiated accretion disks with maximum grain sizes no larger than 1 millimeter fit the SEDs, however, in most cases we cannot confidently rule out smaller maximum grain sizes. Measurements of mass accretion rates, spectra of the 10 μm silicate feature, and/or millimeter-wave observations are needed to better constrain the models. The two objects with dissimilar SEDs exhibit a lack of excess emission shortward of 5-8 μm indicative of evacuated inner holes. Our models constrain the size of the inner hole in object L316 to $R_{in} \sim$ 0.5-1 AU. This is the first brown dwarf seen to exhibit evidence for a transition disk with an AU-scale inner hole. Processes related to planet formation may have contributed to the clearing of the inner disk, either via planetesimal coagulation to asteroid-size bodies or formation of a single "super-Earth". If true, this suggests that planet formation can occur around objects across the full range of stellar and substellar masses, and puts strong constraints on the formation timescale of a few Myr or less. Further models of grain growth and planetesimal coagulation in such environments need to be advanced in order to assess these possibilities, or whether a different clearing mechanism is required.

This work is based in part on observations made with the *Spitzer Space Telescope*, which is operated by the Jet Propulsion Laboratory, California Institute of Technology under NASA contract 1407. Support for this work was provided by NASA through Contract Number 960785 issued by JPL/Caltech. L. A. acknowledges support from CONACyT grant 172854, and P. D. acknowledges grants from DGAPA, UNAM, and CONACyT, México. K. L. was supported by grant NAG5-11627 from the NASA Long-Term Space Astrophysics program.

REFERENCES

Akeson, R. L., Walker, C. H., Wood, K., Eisner, J. A., Scire, E., Penprase, B., Ciardi, D. R., van Belle, G. T., Whitney, B., & Bjorkman, J. E. 2005, ApJ, 622, 440

Allard, F., Hauschildt, P. H., Alexander, D. R., Tamanai, A., & Schweitzer, A. 2001, ApJ, 556, 357

Apai, D., Pascucci, I., Sterzik, M., et al., 2004, A&A, 426, L53

Baraffe, I., Chabrier, G., Allard, F., & Hauschildt, P. H. 1998, A&A, 337, 403

Boss, A. P. 1997, *Science*, 276, 1836

Briceño, C., Luhman, K. L., Hartmann, L., Stauffer, J. R., & Kirkpatrick, J. D. 2002, ApJ, 580, 317

Calvet, N., D'Alessio, P., Hartmann, L., Wilner, D., Walsh, A., & Sitko, M. 2002, ApJ, 568, 1008

Calvet, N., Briceño, C., Hernàndez, J., Hoyer, S., Hartmann, L., Sicilia-Aguilar, A., Megeath, S. T., & D'Alessio, P. 2005a, AJ, 129, 935

Calvet, N., D'Alessio, P., Watson, D. M., et al. 2005b, ApJ, in press

Clarke, C. J., Gendrin, A., & Sotomayor, M. 2001, MNRAS, 328, 485

Chabrier, G., Baraffe, I. Allard, F., & Hauschildt, P. H. 2000, ApJ, 542, 464

Coméron, F., Neuhäuser, R., & Kaas, A. A. 2000, A&A, 359, 269

Coméron, F., Rieke, G. H., Claes, P., Torra, J., & Laureijs, R. J. 1998, A&A, 335, 522

D'Alessio, P., Cantó, J., Calvet, N., & Lizano, S. 1998, ApJ, 500, 411

D'Alessio, P., Calvet, N., Hartmann, L., Lizano, S., & Cantó, J. 1999, ApJ, 527, 893

D'Alessio, P., Calvet, N. & Hartmann, L. 2001, ApJ, 553, 321

D'Alessio, P., Hartmann, L., Calvet, N., et al. 2005, ApJ, 621, 461

Dullemond, C. P. & Dominik, C. 2005, A&A, 434, 971

Furlan, E. et al. 2005, ApJ, 621, L129

Gammie, C. 1996, ApJ, 457, 355

Gordon, K. et al. 2005, PASP, in press

Hartmann, L., Calvet, N., Gullbring, E. & D'Alessio, P. 1998, ApJ, 495, 385

Hollenbach, D., Johnstone, D., Lizano, S., & Shu, F. 1994, ApJ, 428, 654

Jayawardhana, R., Ardila, D. R., Stelzer, B., & Haisch, K. E. 2003a, AJ, 126, 1515

Klein, R., Apai, D., Pascucci, I., Henning, T., & Waters, L. B. F. M. 2003, ApJ, 593, L57

Lada, C. J., et al. 2005, ApJ, submitted

Liu, M. C., Najita, J., & Tokunaga, A. T. 2003, ApJ, 585, 372

Luhman, K. L. 1999, ApJ, 525, 466

Luhman, K. L., Stauffer, J. R., Muench, A. A., Rieke, G. H., Lada, E. A., Bouvier, J., & Lada, C. J. 2003, ApJ, 593, 1093

Luhman, K. L., Lada, C. J., Hartmann, L., et al, ApJL in press

Luhman, K. L., D'Alessio, P., Calvet, N., et al. 2005b, ApJ, 620, L51

Mathis, J. S. 1990, ARA&A, 28, 37

Mathis, J. S., Rumpl, W., & Nordsieck, K. H. 1977, ApJ, 217, 425

Matsuyama, I., Johnstone, D., & Hartmann, L. 2003, ApJ, 582, 893

Meyer, M. R., Calvet, N., & Hillenbrand, L. A. 1997, AJ, 114, 288

Mohanty, S., Jayawardhana, R., & Basri, G. 2005, ApJ, 626, 498

Mohanty, S., Jayawardhana, R., Natta, A., Fujiyoshi, T., Tamura, M., & Barrado y Navascués, D. 2004, ApJ, in press

Muench, A. A., Alves, J., Lada, C. J., & Lada, E. A. 2001, ApJ, 558, L51

Muzerolle, J., Briceño, C., Calvet, N., Hartmann, L., Hillenbrand, L. A., & Gullbring, E. 2000, ApJ, 545, L141

Muzerolle, J., Calvet, N., Hartmann, L., & D'Alessio, P. 2003a, ApJ, 597, L149

Muzerolle, J., D'Alessio, P., Calvet, N., & Hartmann, L. 2004, ApJ, 617, 406

Muzerolle, J., Hillenbrand, L., Calvet, N., Briceño, C., & Hartmann, L. 2003b, ApJ, 592, 266

Muzerolle, J., Luhman, K., Briceño, C., Hartmann, L., Calvet, N. 2005, ApJ, 625, 906

Najita, J., Carr, J. S., & Mathieu, R. D. 2003, ApJ, 589, 931

Natta, A. & Testi, L. 2001, A&A, 376, L22

Natta, A., Testi, L., Comerón, F., Oliva, E., D'Antona, F., Baffa, C., Comoretto, G., & Gennari, S. 2002, A&A, 393, 597

Natta, A., Testi, L., Muzerolle, J., Randich, S., Comerón, F., & Persi, P. 2004, A&A, 424, 603

Nelson, R. P., Papaloizou, J. C. B., Masset, F., & Kley, W. 2000, MNRAS, 318, 18

Padoan, P., & Nordlund, Å. 2002, ApJ, 576, 870

Papovich, C. et al. 2004, ApJS, 154, 70

Plavchan, P., Jura, M., & Lipscy, S. J. 2005, ApJ, in press

Quillen, A. C., Blackman, E. G., Frank, A., & Varnière, P. 2004, ApJ, 612, L137

Reipurth, B. & Clarke, C. 2001, AJ, 122, 432

Rice, W. K. M., Wood, K., Armitage, P. J., Whitney, B. A., & Bjorkman, J. E. 2003, MNRAS, 342, 79

Rieke, G. H. et al. 2004, ApJS, 154, 25

Ruden, S. P. 2004, ApJ, 605, 880

Sicilia-Aguilar, A. et al. 2005, ApJ, submitted

Sterzik, M. F., Pascucci, I., Apai, D., van der Bliek, N., & Dullemond, C. P. 2004, A&A, 427, 245

White, R. J. & Basri, G. 2003, ApJ, 582, 1109 (WB03)

Weidenschilling, S. 1997, Icarus, 127, 290

Table 1. The Low-Mass/Substellar 24 μm Sample

ID	α(J2000)	δ(J2000)	Sp. Type	A_V	M_* ($M_\odot$)	R_* ($R_\odot$)	$L_{\rm bol}$ ($L_\odot$)
L199[a]	03:43:57.22	32:01:33.9	M6.5	9.2	0.08	1.15	0.087
L205[b]	03:44:29.80	32:00:54.6	M6	2.3	0.1	1.15	0.095
L291[c]	03:44:34.05	32:06:56.9	M7.25	1.0	0.05	0.74	0.032
L316[c]	03:44:57.73	32:07:41.9	M6.5	1.2	0.075	0.71	0.033
L1707[a]	03:43:47.63	32:09:02.7	M7	1.0	0.06	0.53	0.017
L30003[a]	03:43:59.17	32:02:51.3	M6	8.0	0.1	0.54	0.021

Note. — Object IDs and properties have the following references: [a]Lada et al. in preparation; [b]Luhman (1999); [c]Luhman et al. (2003).

Table 2. *Spitzer* Fluxes

ID	$F_{3.6}$	$F_{4.5}$	$F_{5.8}$	F_8	F_{24}
L199	4.87 ± 0.28	4.08 ± 0.18	3.92 ± 0.22	3.84 ± 0.12	5.58 ± 0.24
L205	6.12 ± 0.06	5.81 ± 0.13	6.06 ± 0.31	6.79 ± 0.18	10.58 ± 0.32
L291	4.73 ± 0.09	4.25 ± 0.10	3.90 ± 0.14	4.35 ± 0.22	5.35 ± 0.23
L316	2.53 ± 0.02	1.79 ± 0.06	1.25 ± 0.08	1.02 ± 0.16	6.57 ± 0.22
L1707	1.79 ± 0.03	1.62 ± 0.02	1.38 ± 0.07	1.58 ± 0.06	2.45 ± 0.09
L30003	0.75 ± 0.04	1.03 ± 0.03	1.30 ± 0.12	2.27 ± 0.13	3.06 ± 0.35

Note. — Fluxes in mJy. MIPS 24 μm flux uncertainties are the formal errors from the PSF-fitting procedure, and do not include the 10% calibration uncertainty.

Table 3. Disk Model Parameters

Object	T_{wall} (K)	log $\dot{M}$	cos(i)	R_{wall} (R_*)	H_{wall} (R_*)	H_{wall}^{pred} (R_*)
			$a_{max} = 0.25$ μm			
L199	1400	-12	0.9	4.5	0.1	0.22
L205	1400	-11	0.5	4.7	0.2	0.23
L291	1400	-11	0.5	4.1	0.4	0.25
L316	200	-12	0.8	276.2	8.0	···
L1707	1400	-11	0.5	4.1	0.2	0.26
L30003	500	-12	0.5	45.5	2.0	1.3
			$a_{max} = 1$ mm			
L199	1400	-10	0.5	4.5	0.1	0.22
L205	1400	-10	0.8	4.7	0.2	0.23
L291	1400	-10	0.9	4.1	0.6	0.26
L316	250	-12	0.5	165.4	8.0	···
L1707	1400	-10	0.9	4.1	0.3	0.27
L30003	500	-12	0.5	45.5	2.0	1.3

Note. — $\dot{M}$ in units of $M_\odot\,\mathrm{yr}^{-1}$. R_{wall} is the radius of the wall at the inner edge of the dust disk, corresponding to the dust sublimation radius for all except L316 and L30003. H_{wall} is the height of the wall that provides the best fit to the observed SEDs; uncertainties in the exact level of the underlying photosphere at $\lambda \sim 2-8$ μm yield typical uncertainties on H_{wall} of about 0.1 R_* (0.5-1 R_* for the large holes). H_{wall}^{pred} is the predicted wall height for $a_{max} = 0.25$ μm according to the treatment of Muzerolle et al. (2004).

Fig. 1.— Central $\sim$ 30'x30' portion of the 24 μm map of IC 348. The positions of all known members with spectral types M6 or later are marked with green diamonds; those with measurable 24 μm fluxes are shown with yellow boxes. (See PNG file.)

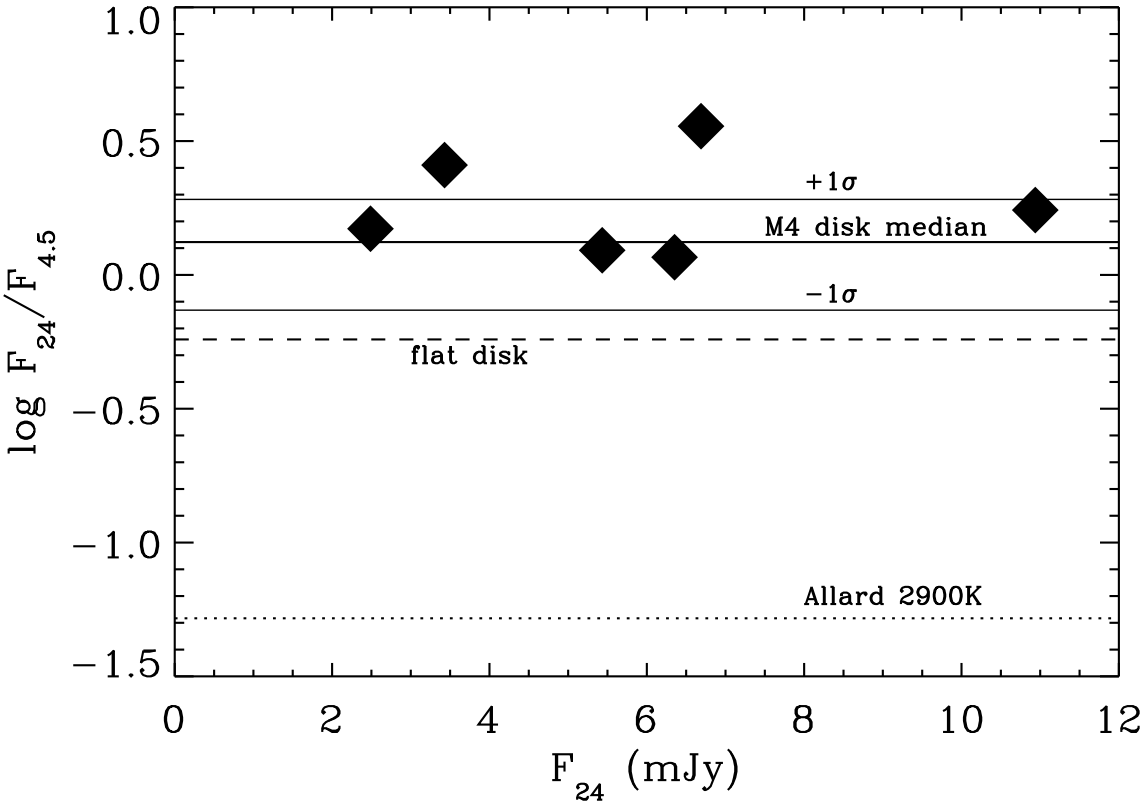

Fig. 2.— The ratio of fluxes at 24 μm and 4.5 μm as a function of the 24 μm flux for the 6 low-mass/substellar 24 μm detections (solid diamonds), all dereddened using A_V determined empirically from optical photometry and spectral types (Luhman et al. 2003) and the Mathis (1990) reddening law. The theoretical flux ratio for an M6.5 photosphere, derived from an Allard et al. (2001) AMES-COND model for T_{eff} = 2900 K, is shown with the dotted line. The dashed line shows the flux ratio upper limit for a spectral slope $\lambda F_\lambda \propto \lambda^{-4/3}$ corresponding to a geometrically thin, optically thick flat disk, assuming negligible contribution to the 4.5 μm flux from the photosphere. The solid line shows the median slope and the dot-dashed lines the $\pm 1\sigma$ values for $\sim$ 15 members of IC 348 with spectral types M4-M5 with excesses indicative of optically thick disks, as defined in Lada et al. (2005).

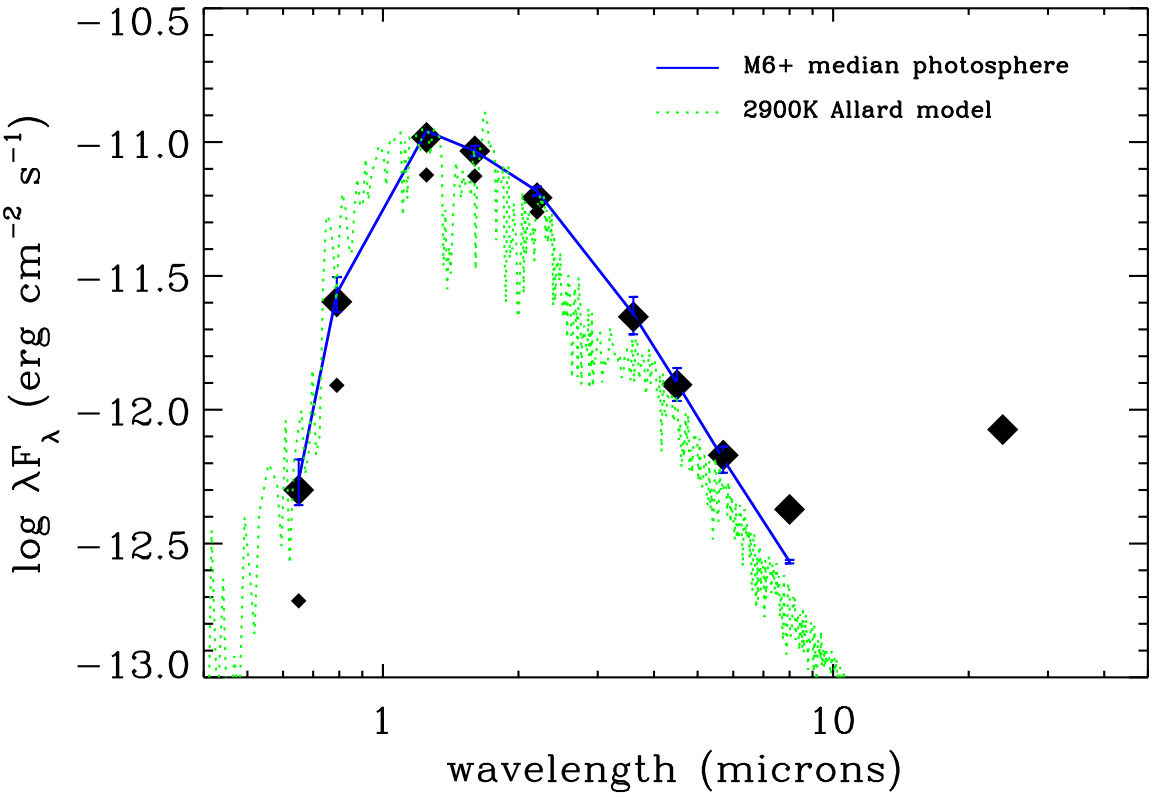

Fig. 3.— Observed SED for the substellar object L316 (diamonds). Ground-based optical and near-infrared photometry are taken from Luhman et al. (2003), IRAC data from Lada et al. (2005) and Luhman et al. (2005). All fluxes have been dereddened using the observed A_V and the reddening law of Mathis (1990) (large diamonds); the original reddened fluxes are also shown (small diamonds). The median SED and 1-sigma dispersion for 8 IC 348 members with spectral types later than M6 which lack infrared excess, normalized to the L316 SED at J, are shown with the solid line and error bars (from Lada et al. 2005). For further comparison, a photospheric model with T_{eff} = 2900 K from Allard et al. (2001) is shown with the dotted line. Note the systematically lower flux of this model compared to the empirical photosphere at the first 3 IRAC bands, which might cause a false inference of excess emission if one relied only on the model to represent the intrinsic substellar photosphere.

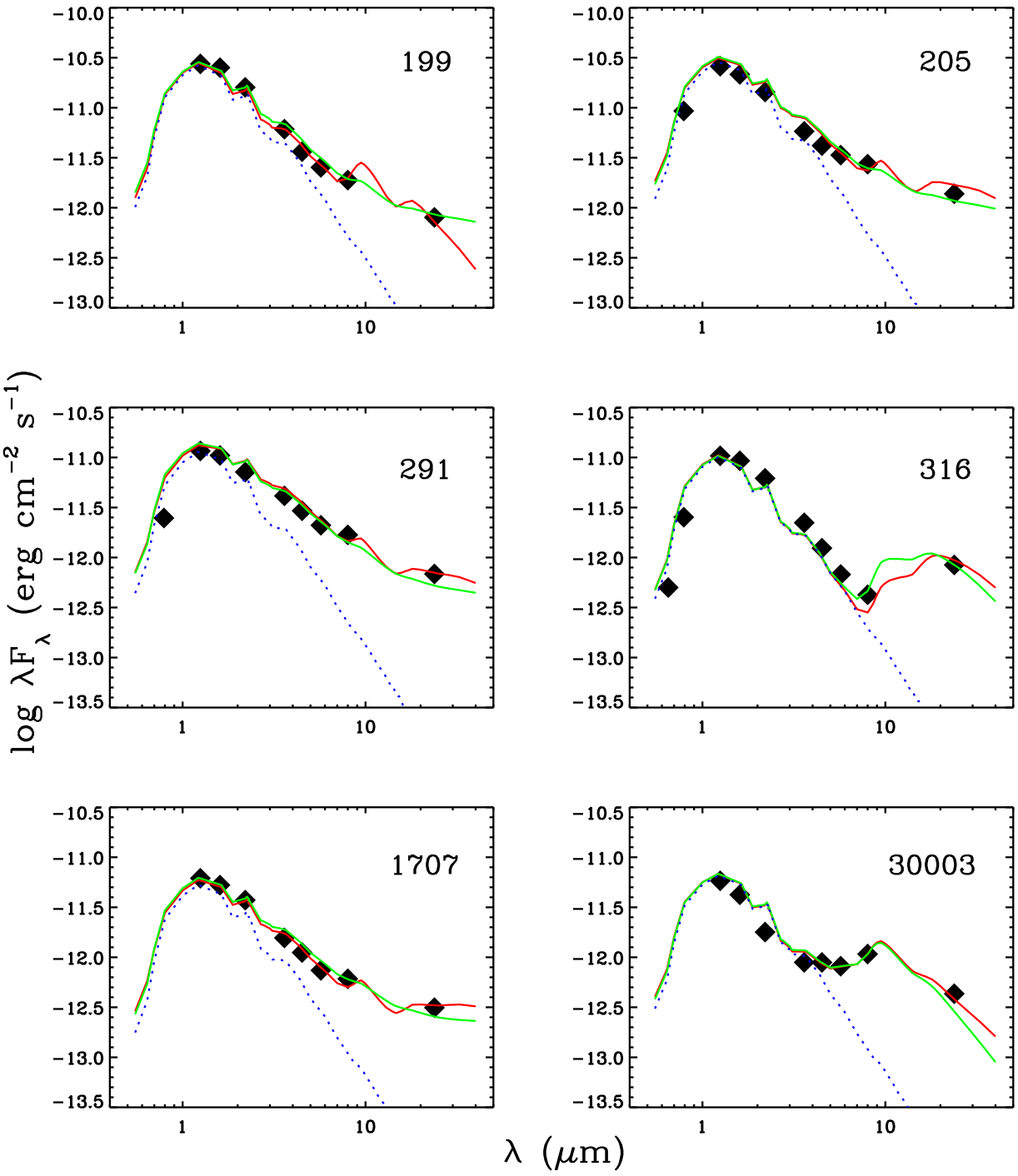

Fig. 4.— Observed SEDs for all 24 μm detections with spectral types M6 or later (squares). Ground-based optical and near-infrared photometry from Luhman et al. (2003) and Luhman et al. (2005, in preparation), IRAC data from Lada et al. (2005) and Luhman et al. (2005). All fluxes have been dereddened using the observed A_V and the reddening law of Mathis (1990). Best-fit disk models with maximum grain size a_{max} = 0.25 μm and 1 mm are shown with the red and green solid lines, respectively. These models include a photospheric component using the theoretical models of Allard et al. (2001) appropriate for the spectral type of each object, smoothed versions of which are shown separately with the blue dotted

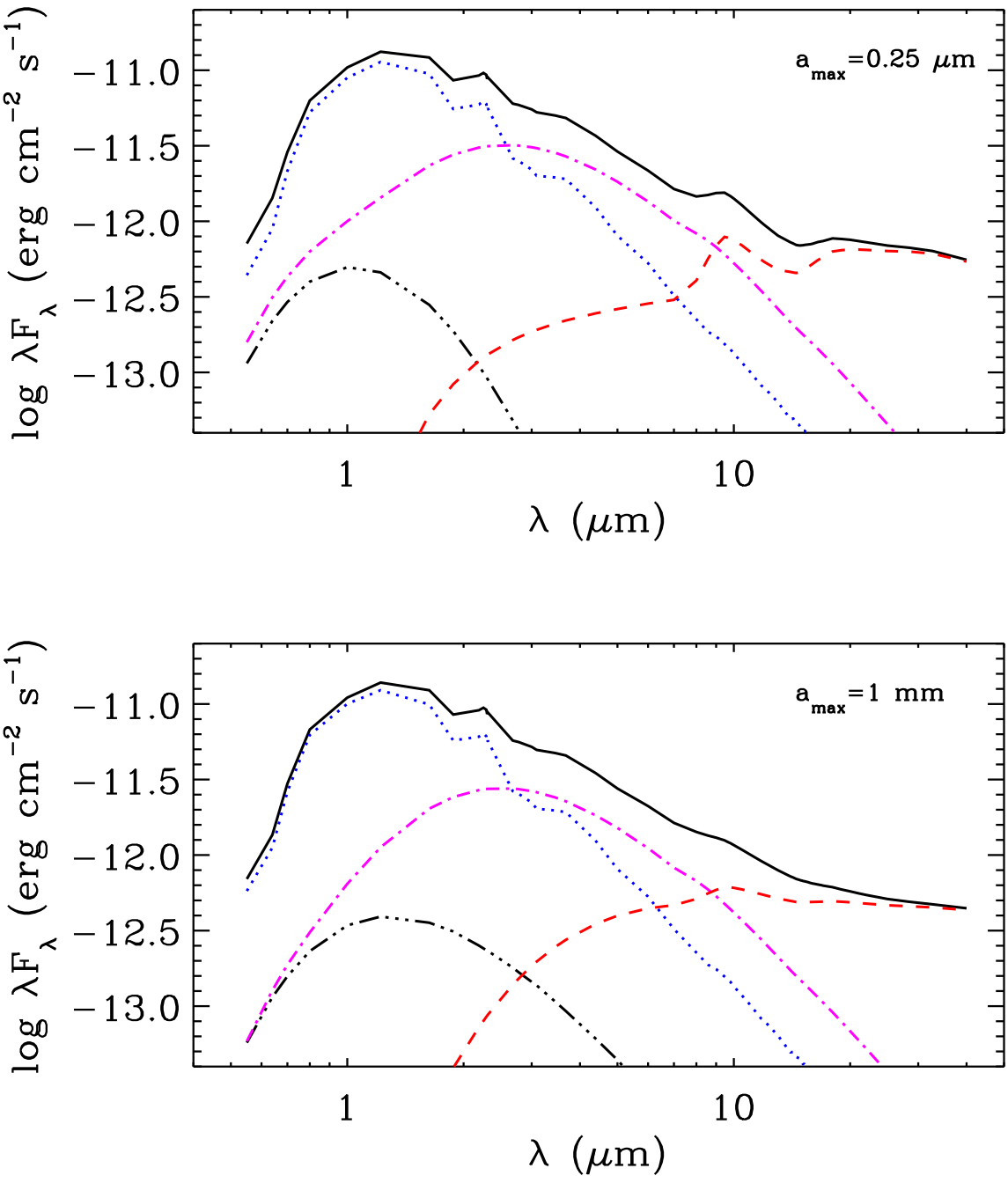

Fig. 5.— Brown dwarf disk models for L291 parameters: (top) for a_{max} = 0.25 μm ; (bottom) for a_{max} = 1 mm. Blue dotted lines are Allard et al. (2001) model atmospheres with T_{eff} = 2900 K, $log(g)$ = 3.5; red dashed lines are the emission from the disk surface; magenta dash-dotted lines are the emission from the inner disk wall; black dash-dot-dot lines are the contribution from scattered light; solid black lines are the total emission.

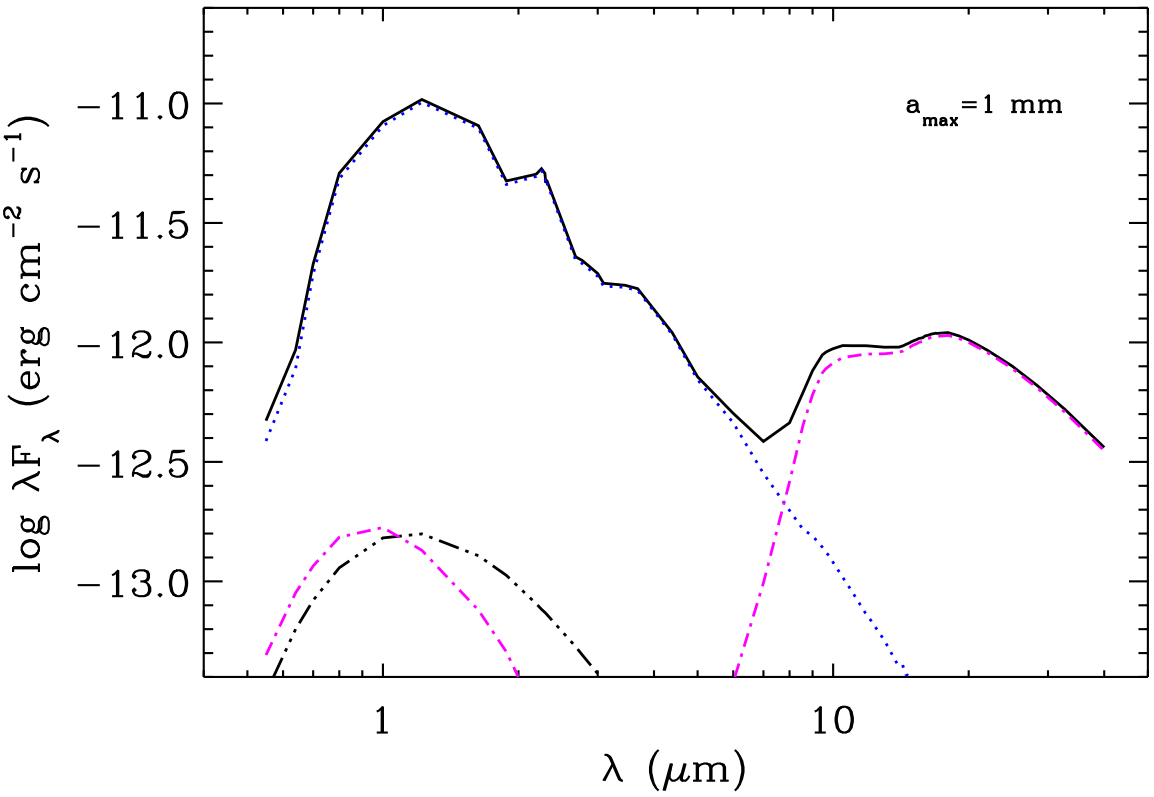

Fig. 6.— Same as in Figure 5 with $a_{max} = 1$ mm for the case of a large (~ 1 AU) inner disk hole.

This figure "f1.png" is available in "png" format from:

http://arXiv.org/ps/astro-ph/0603104v1